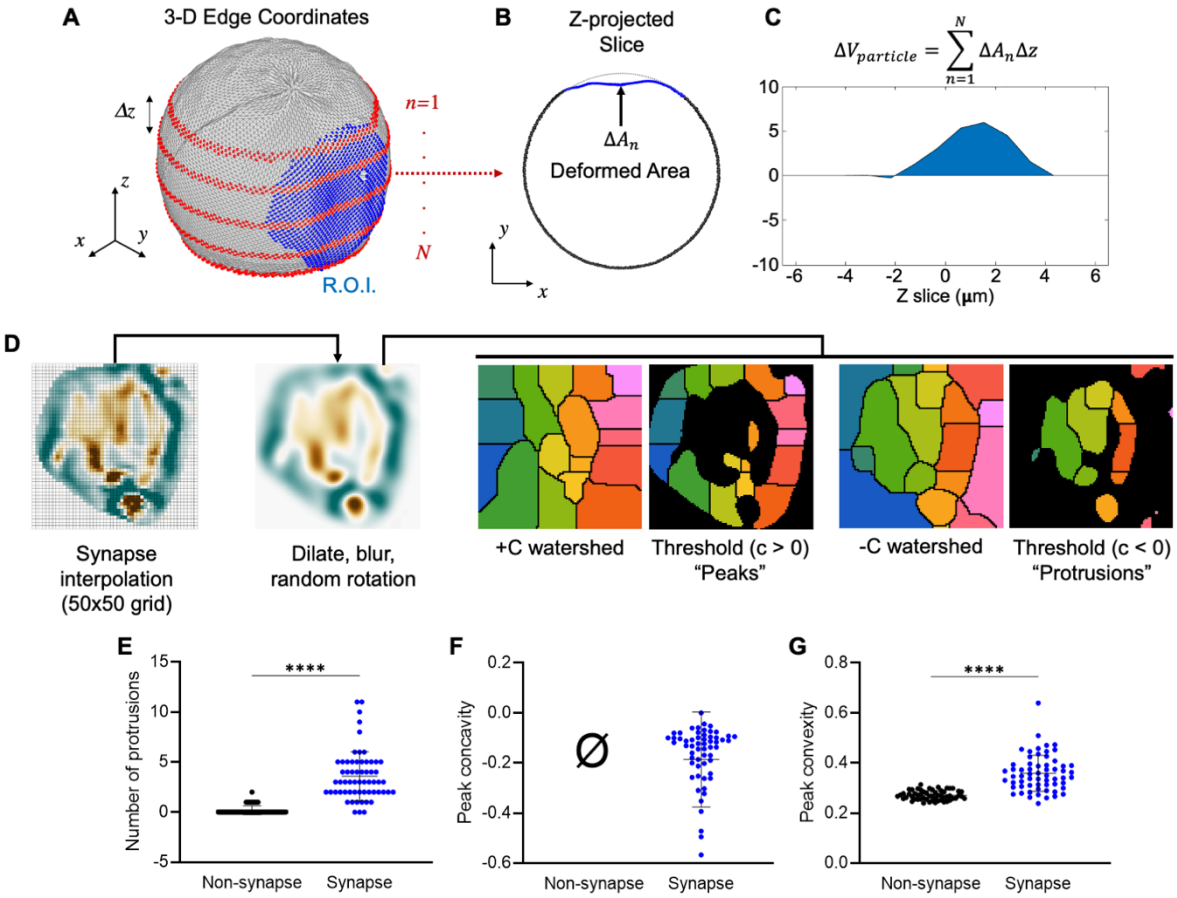

Figure S1. CTLs form compressive contacts containing local indentations and reliefs. (A-C) Protocol for determining deformation volume. (A) Contacts were positioned orthogonally to x- and y-axes and divided into 10 equal sections along the z-axis. (B) Each section was fit to a circle to determine deformed area. (C) These areas were then integrated over all z-sections. (D) To identify indentations and reliefs, blurred and dilated topographies were subjected to watershedding followed by intensity thresholding. Curvature values were then extracted from the demarcated features. (E) Number of synaptic indentations in CTL synapses and non-synapse controls. (F-G) Peak indentation concavity (F) and peak relief convexity (G) within CTL synapses and non-synapse controls. Non-synapse controls lacked sufficient indentations for concavity scoring. **** denotes P ≤ 0.0001, calculated by unpaired Welch's t-test. Error bars indicate SD.

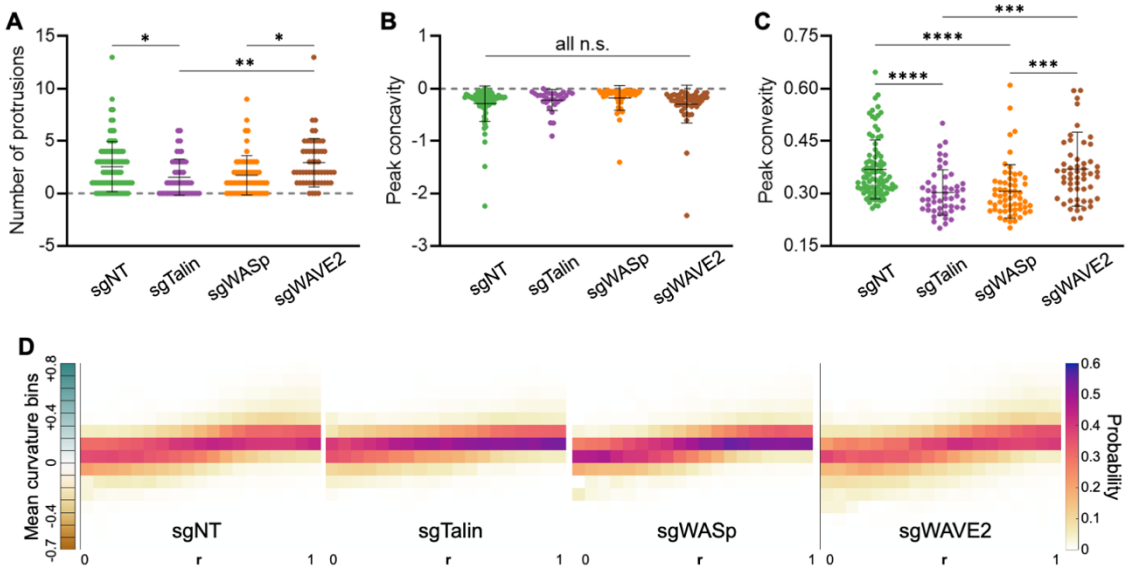

Figure S2. Compressive strength and protrusive activity distinguish lytic from non-lytic synapses. (A) Number of synaptic indentations formed by CTLs expressing the indicated sgRNAs. (B-C) Peak indentation concavity (B) and peak relief convexity (C) within synapses formed by CTLs expressing the indicated gRNAs. *, **, ***, and **** denote $P \leq 0.05$, $P \leq 0.01$, $P \leq 0.001$, and $P \leq 0.0001$, respectively, calculated by multiple t-testing with Tukey's correction. Error bars indicate SD. (D) Radial mean curvature plots derived from CTLs expressing the indicated sgRNAs. (n = 89 sgNT, 50 sgTalin, 60 sgWASp, and 54 sgWAVE2 CTLs).

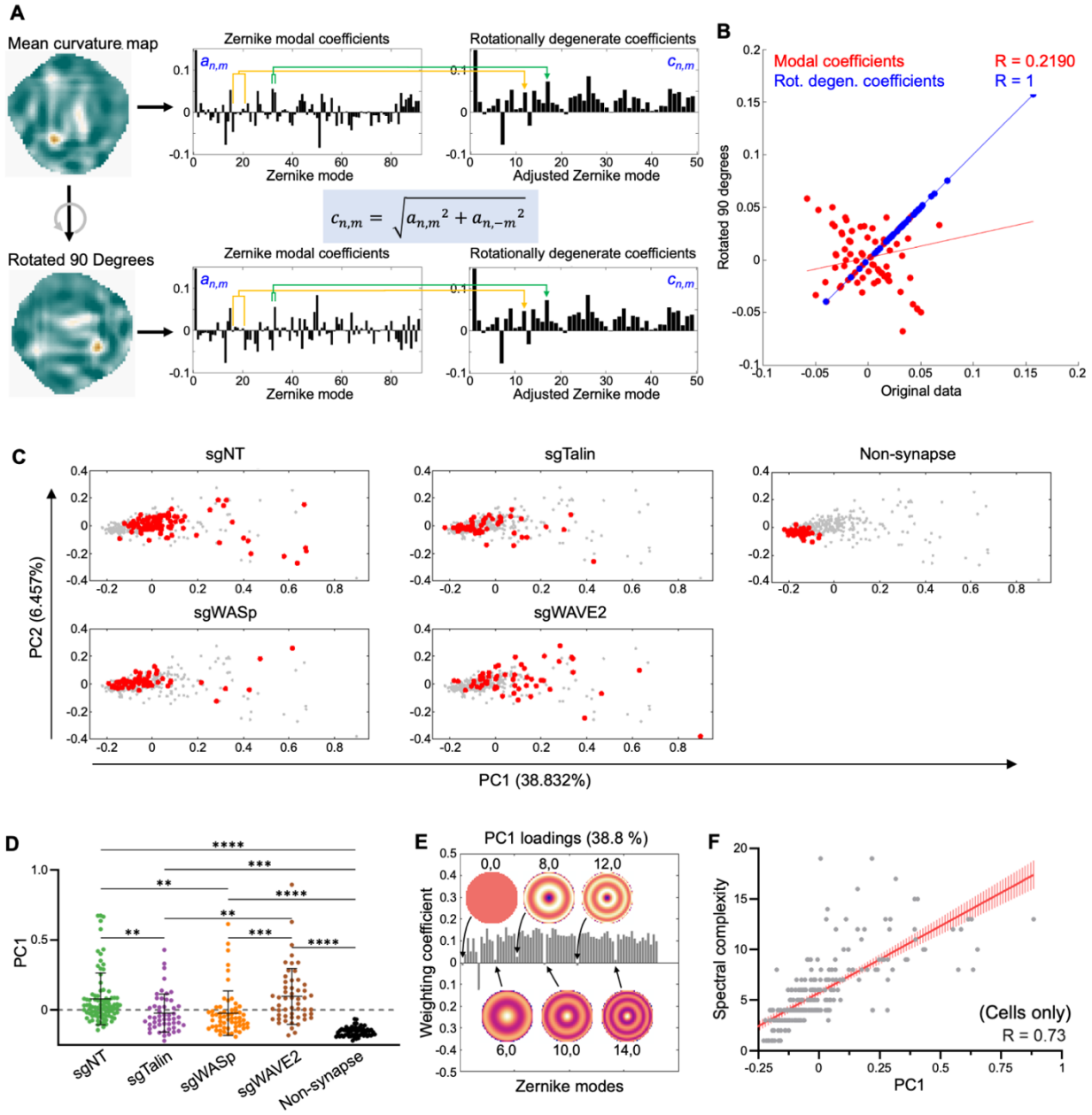

Figure S3. Z-pattern spectral analysis links cytolytic activity to topographical complexity and asymmetry. (A) Identical topographies related by rigid body rotation generate distinct Zernike spectra. Combining azimuthally related Zernike coefficients *via* their quadrature sum eliminates this spurious distinction. (B) Scatter plot comparing correlations between the modal coefficients before (red, R = 0.22) and after (blue, R = 1) azimuthal combination. (C) Topographies of the indicated CTL synapses, together with non-synapse controls, were transformed into rotationally degenerate Z-pattern spectra and then visualized by PCA. Plots show each of the experimental groups in red overlaid onto the rest of the data set in gray. (D) PC1 values for each experimental group. *, **, ***, and **** denote P ≤ 0.05, P ≤ 0.01, P ≤ 0.001, and P ≤ 0.0001,

respectively, calculated by multiple t-testing with Tukey's correction. Error bars indicate SD. (E) Zernike polynomial loading (coefficient breakdown) of PC1 in this data set. Modes with particularly low contributions are indicated. (F) Scatter plot relating PC1 to spectral complexity for all topographies in this data set (with Pearson correlation coefficient R), excluding the non-synapse controls. Regression line (red) is plotted with bars denoting the 95 % confidence interval.

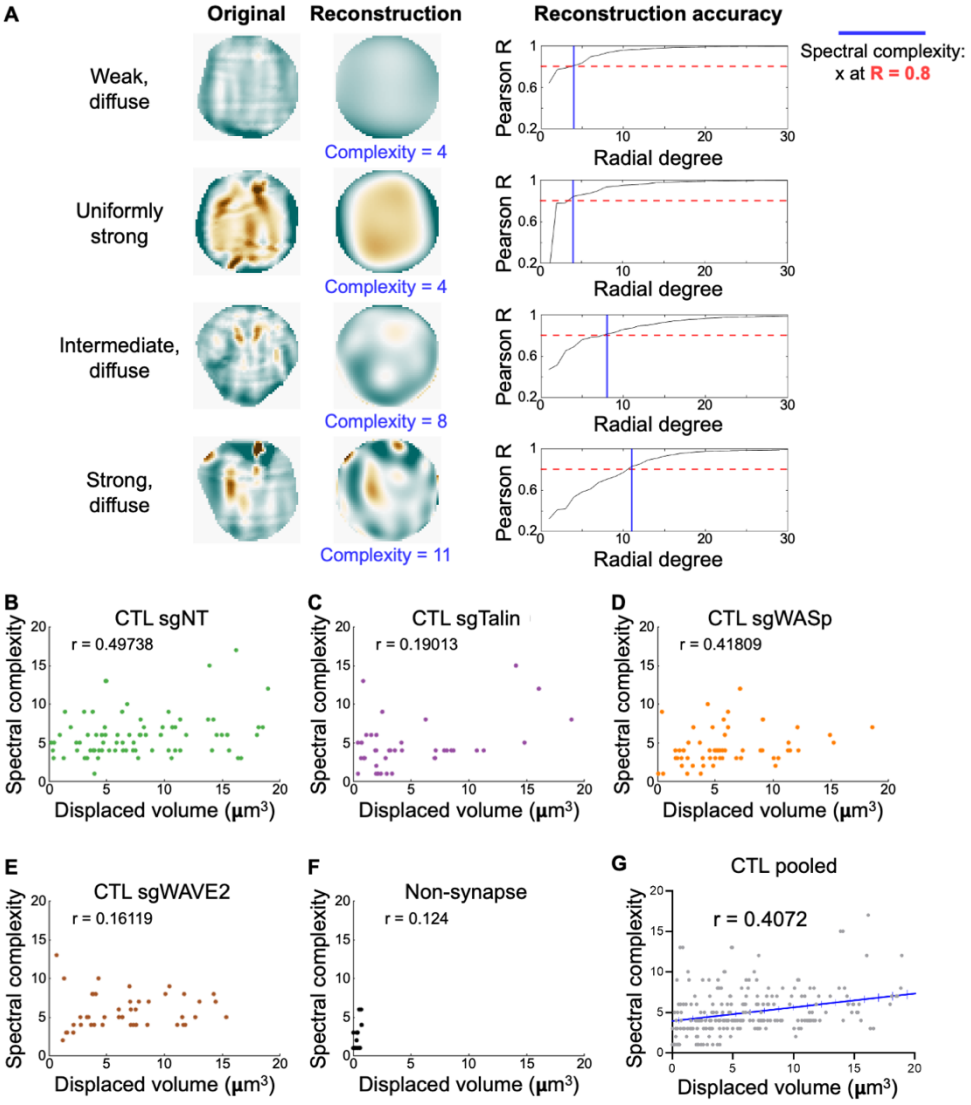

Figure S4. Determination of spectral complexity. (A) Topographies representing four different types of synapse mechanics were subjected to Zernike reconstruction with different numbers of radial degrees (sets of polynomials). Left, original curvature maps of the four topographies. Right, graphs relating the quality of reconstruction (determined by Pearson R) to the number of Zernike orders used. Blue lines indicate the order at which Pearson R = 0.8, which we define as *spectral complexity*. Center, the reconstructed image at R ≤ 0.8, with the corresponding spectral complexity metric. (B-F) Scatterplots relating net particle compression to spectral complexity for sgNT (B), sgTalin (C), sgWASp (D), sgWAVE2 (E), and non-synapse control (F) topographies. (G) Scatter plot relating net particle compression to spectral complexity for all topographies in this data set (with Pearson R), excluding the non-synapse controls. Regression line (blue) is plotted with bars indicating the 95 % confidence interval.

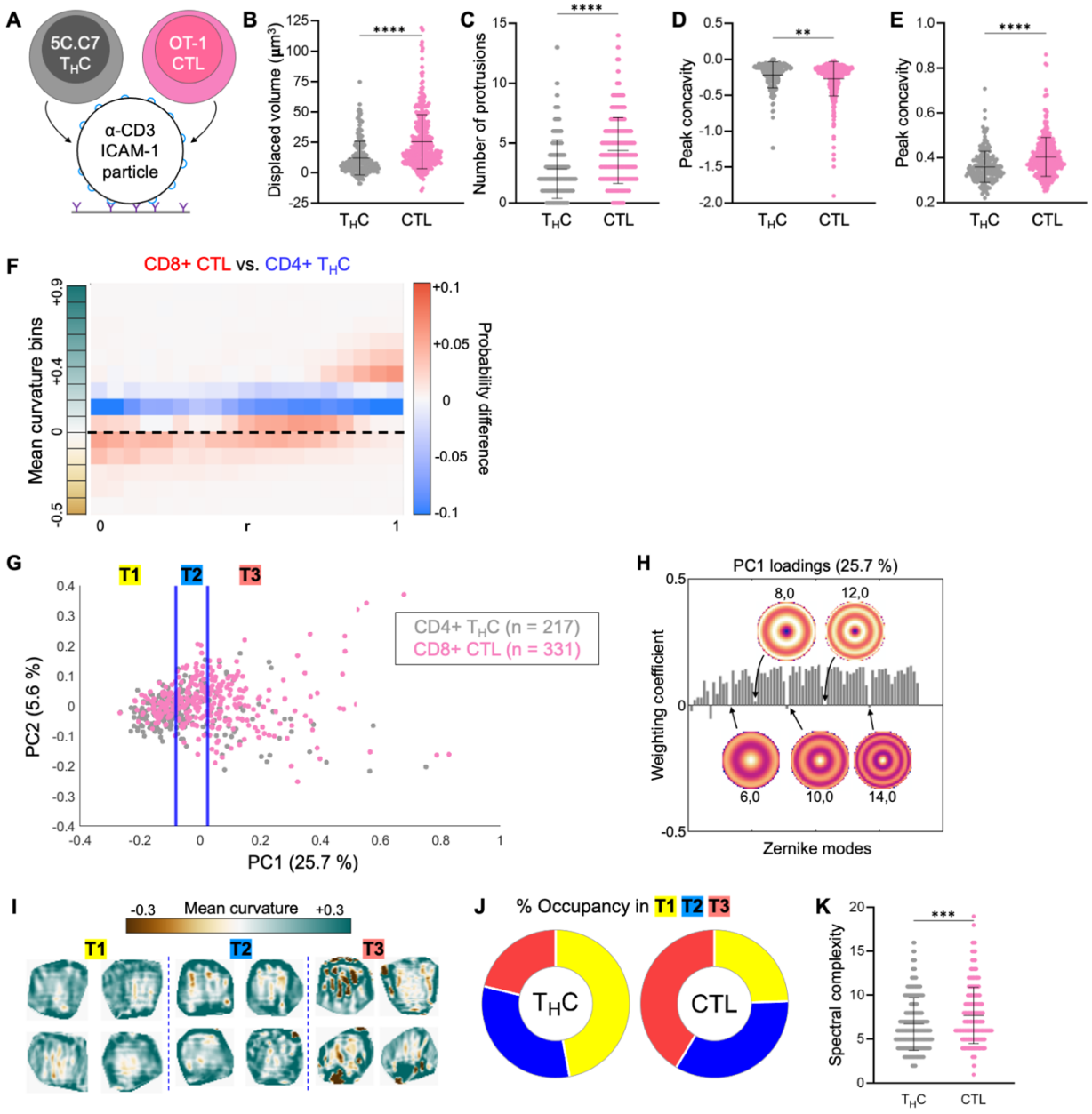

Figure S5. CTLs induce stronger and more complex distortions than T_HCs. (A) OT-1 CTLs and 5C.C7 T_HCs were cultured in parallel and imaged together with DAAM particles coated with anti-CD3ε antibody and ICAM-1. (B-E) Quantification of particle compression (B), protrusion number (C), peak indentation concavity (D), and peak relief convexity (E) within synapses formed by the indicated T cells. (F) Difference plot of radial curvature distribution, colored red and blue for over-representation of CTLs and T_HCs, respectively. Dotted line indicates 0 curvature (flat). (G) CTL and T_HC topographies were represented as Z-pattern spectra and visualized by PCA. Data points were separated into terciles (indicated by the blue lines) for downstream analysis. A) Zernike polynomial loading of PC1. Modes with particularly low contributions are highlighted. (I)

Cropped views of representative synapses from each tercile in G. (J) Distribution of CTL and T_HC synapses across the terciles of PC space. (K) Spectral complexity comparison of CTLs and T_HCs. **, ***, and **** denote P ≤ 0.01, P ≤ 0.001, and P ≤ 0.0001, respectively, calculated by unpaired Welch's t-test. All error bars indicate SD.

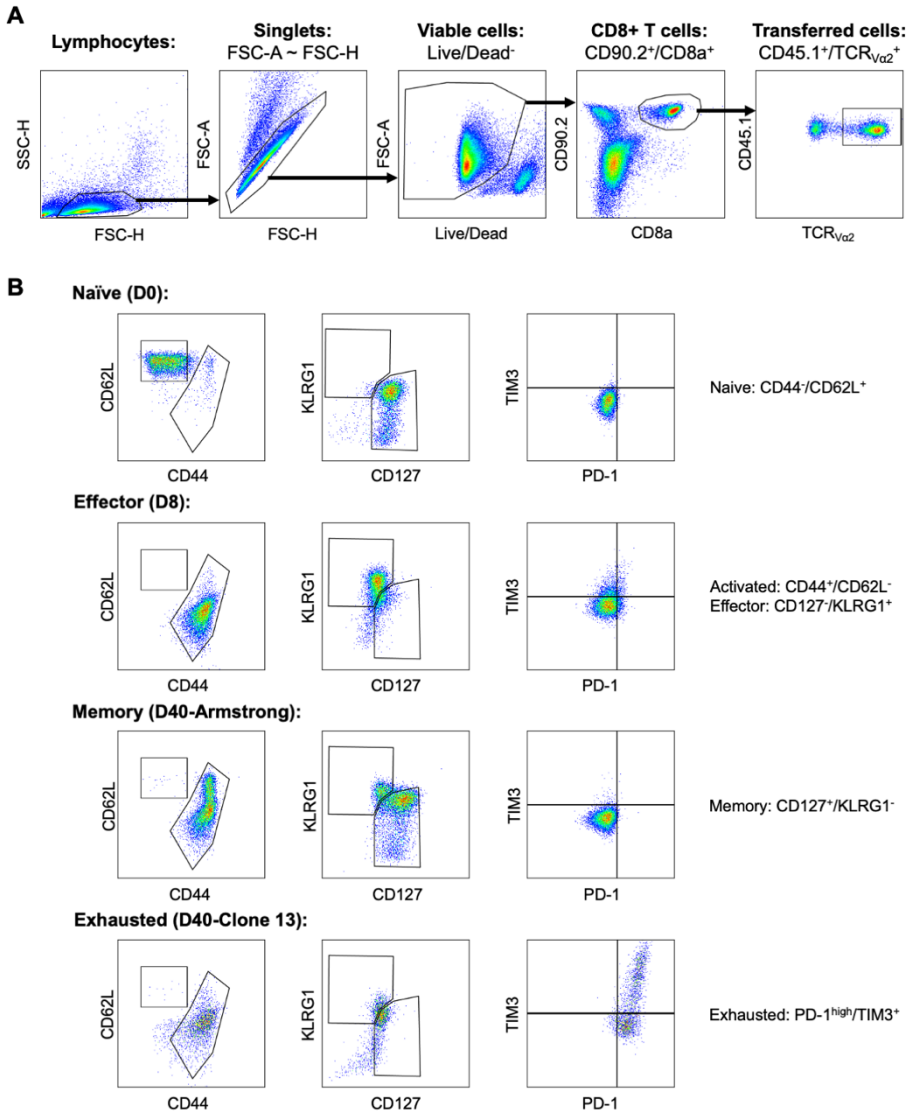

Figure S6. Purification of *in vivo* differentiated CD8⁺ T cells. (A) sorting strategy to extract CD45.1 P14 T cells from spleen. (B) representative phenotyping of T_n, T_{eff}, T_{mem}, and T_{exh} P14 cells. Leftmost panels distinguish naïve from antigen experienced T cells. Central panels distinguish terminal effectors from naïve and memory-like cells. Rightmost panels identify exhausted cells.

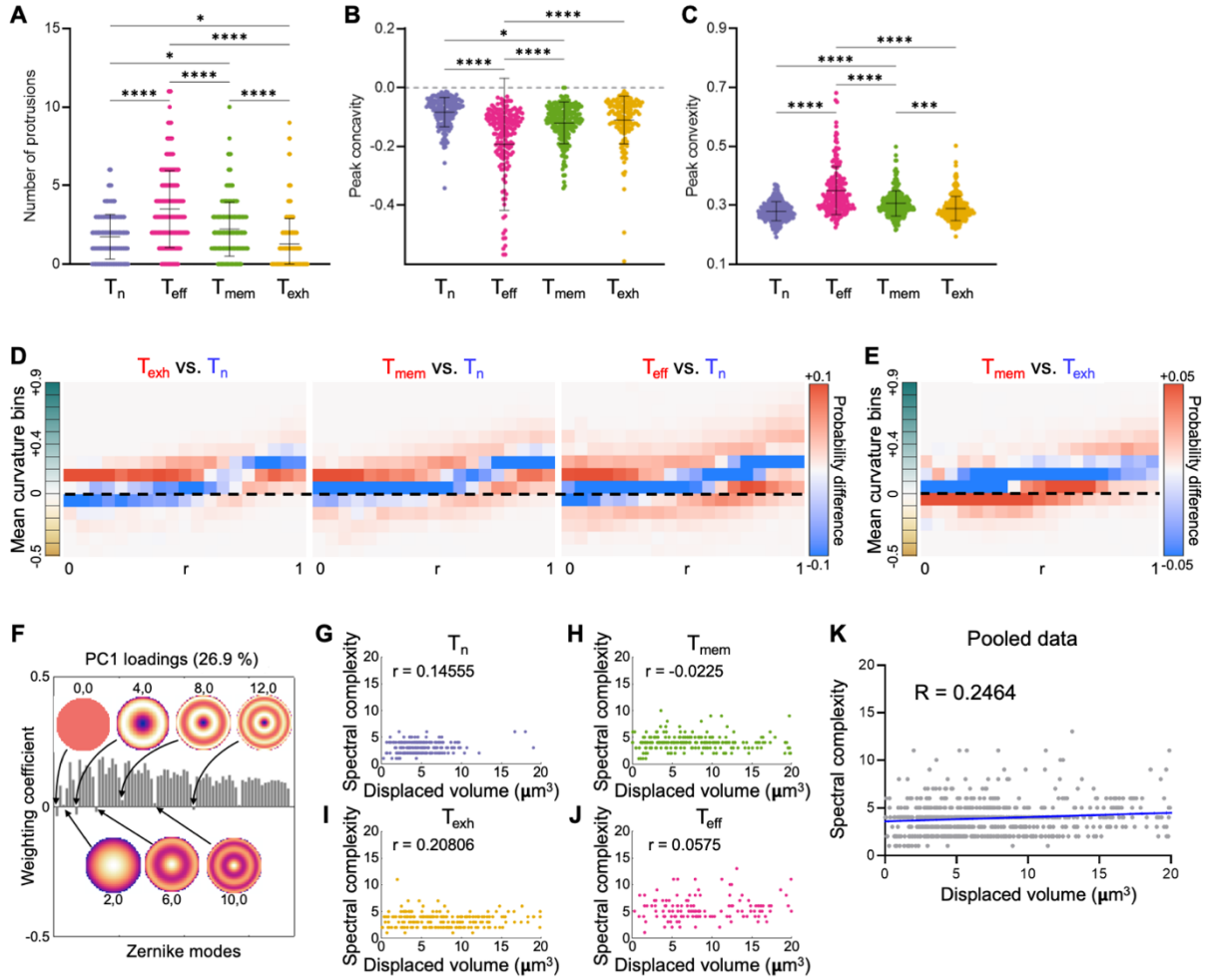

Figure S7. Mechanical activity distinguishes CD8⁺ T cell differentiation states. (A) Number of synaptic indentations formed by the indicated T cell subsets. (B-C) Peak indentation concavity (B) and peak relief convexity (C) within synapses formed by the indicated T cell subsets. *, **, ***, and **** denote $P \leq 0.05$, $P \leq 0.01$, $P \leq 0.001$, and $P \leq 0.0001$, respectively, calculated by multiple t-testing with Tukey's correction. Error bars denote SD. (D) Difference plots of radial curvature distribution, obtained by subtracting the mean curvature distributions of T_{exh} (left), T_{mem} (center), and T_{eff} (right) cells from the mean curvature distribution of T_n cells. Curvature domains are colored blue and red if they are over-represented in T_n cells and their differentiated counterpart, respectively. (E) Difference plot obtained by subtracting the mean curvature distribution of T_{mem} cells from the mean curvature distribution of T_{exh} cells. Curvature domains are colored blue and red if they are over-represented in T_{exh} and T_{mem} cells, respectively. In D and E, the dotted line indicates 0 curvature (flat). (F) T_n, T_{exh}, T_{mem}, and T_{eff} topographies were transformed into Z-pattern spectra (PCA in Fig. 5C). Graph shows Zernike polynomial loading of PC1. Modes with particularly low contributions are highlighted. (G-J) Scatter plots relating net particle compression

to spectral complexity for T_n (G), T_{mem} (H), T_{exh} (I), and T_{eff} (J) topographies. (K) Scatter plot relating net particle compression to Spectral complexity for all topographies in this data set (with Pearson R). Regression line (blue) is plotted with bars denoting the 95 % confidence interval.

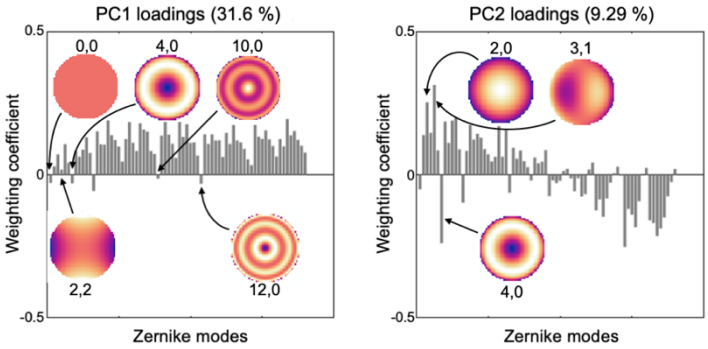

Figure S8. Radial asymmetry is a major source of pattern variation between distinct immune cell types. BMDM and CTL topographies were transformed into Z-pattern spectra and then visualized by PCA (Fig. 6I). Left, Zernike polynomial loading for PC1. Modes with particularly low contributions are highlighted. Right, Zernike polynomial loading for PC2. Modes with major contributions of global concavity/convexity [e.g., Zernike polynomial (2,0) and (4,0)] are indicated.

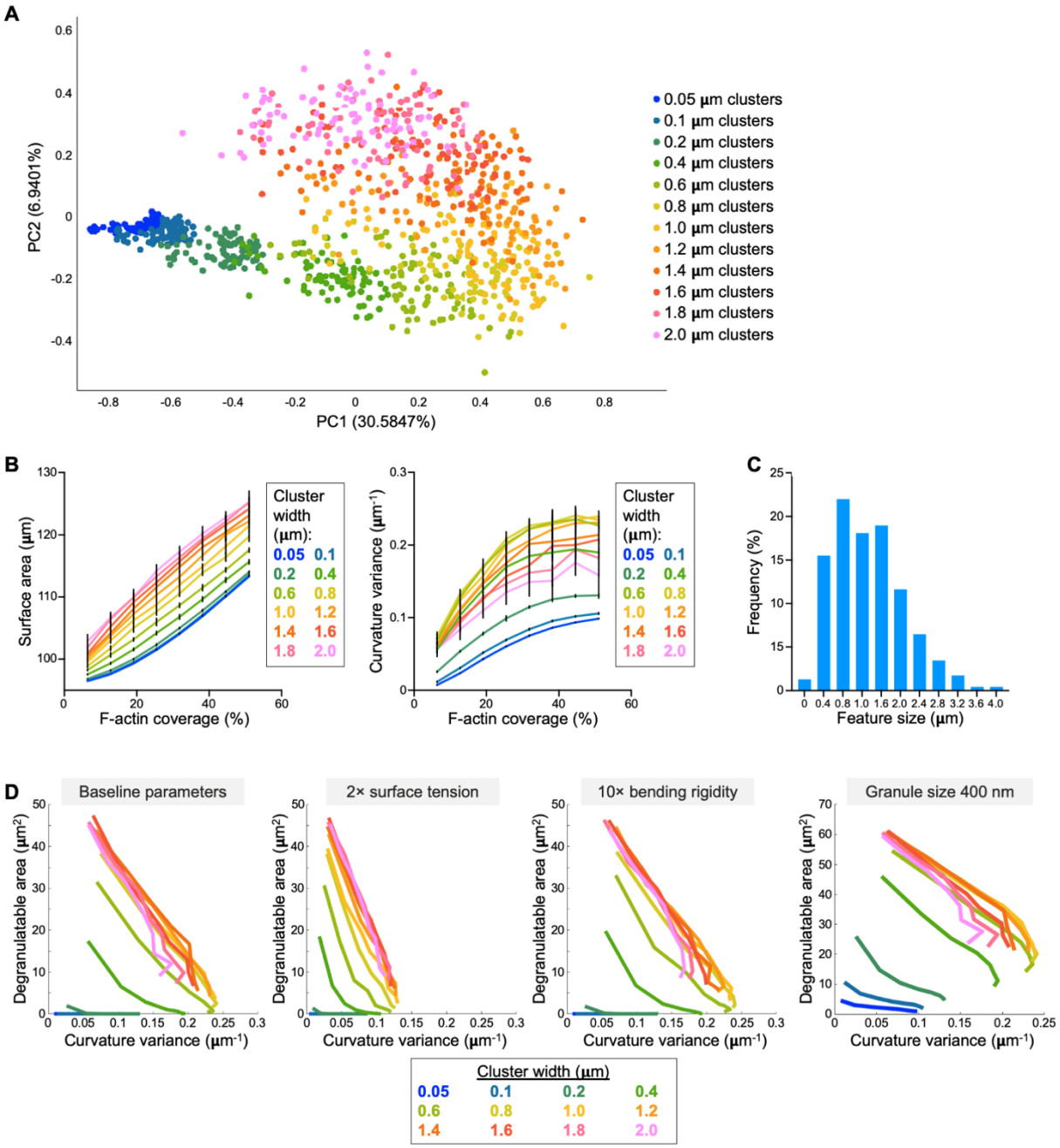

Figure S9. *In silico* modeling of the cytolytic mechanotype. (A) Simulated synapse topographies were transformed into Z-pattern spectra and then visualized by PCA. Topographies are color-coded based on F-actin cluster size. (B) Surface strain, measured by total surface area (left) and curvature variance (right), plotted as a function of F-actin coverage. Lines indicate different F-actin cluster sizes. Error bars denote SD, calculated from 10 replicate simulations. (C) Histogram showing the distribution of concave synapse feature size, derived from P14 day 8 T_{eff} cells (N = 68). For each measurement, the major and minor axes of the feature in question were averaged. (D) 2-D plots of the surface distortion, measured by curvature variance, graphed

against degranulatable area. Each colored line encompasses the mean values of all simulations performed at the indicated F-actin cluster size over all F-actin coverage regimes. The leftmost graph was generated using baseline simulation and analysis parameters (see Methods). Other graphs depict the consequences of specific changes to these parameters.

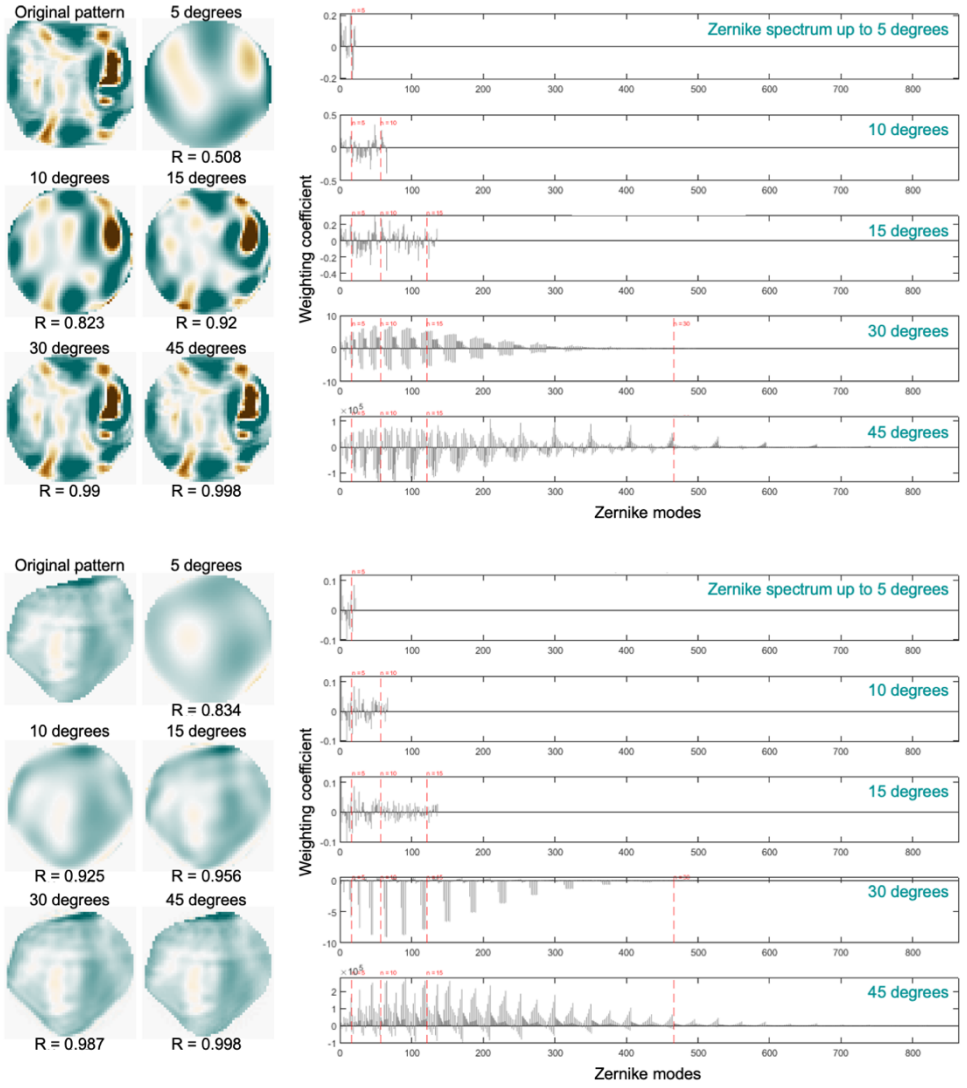

Figure S10. Zernike reconstruction of synapse topographies. Two representative topographies are shown to the left along with reconstructions generated using increasing degrees of Zernike polynomials. Note that Pearson R value improves asymptotically with increasing degree number. Right, spectral representations of each of the reconstructions shown to the left.

Movie Legends

Movie S1. CTLs compress and micropattern target DAAM particles. OT-1 CTLs transduced retrovirally with Lifeact-eGFP were combined with 300-Pa DAAM particles bearing surface H-2K^{b}-OVA and ICAM-1, and imaged every 15 seconds (video is a 150× time-lapse). Top left, a Z-projection of the fluorescence imaging data. Lifeact-eGFP is shown in green and the DAAM particle in magenta. Time in HH:MM:SS is indicated. Top middle: world-map projection of particle shape. x- and y-axes are the polar angles theta and phi, respectively (see Fig. 1C). Red zones represent particle compression against the blue background, which indicates the unindented particle radius. Top right: Topographic map of the particle. Positive and negative curvature are denoted by blue-green and gold, respectively. Bottom row: cross-sectional outline (left) and radii about the cross section (right), showing particle compression and texturing.

Movie S2. The mechanical configuration of the synapse is established in ~5 minutes. OT-1 CTLs transduced retrovirally with Lamp1-eGFP were combined with 300-Pa DAAM particles bearing surface anti-CD3ε (145-2C11) and ICAM-1, and imaged every minute (video is 120×). Top left, a Z-projection of the fluorescence imaging data. Lamp1-eGFP is shown in green and the DAAM particle in pink. Time in minutes is indicated. Top middle: world-map projection of particle shape. x- and y-axes are the polar angles theta and phi, respectively (see Fig. 1C). Red zones represent particle compression against the blue background, which indicates the unindented particle radius. Top right: Topographic map of the particle. Positive and negative curvature are denoted by blue-green and gold, respectively. Bottom row: cross-sectional outline (left) and radii about the cross section (right), showing particle compression and texturing. Contact begins at t = 4 min, and full compression is effected on the DAAM particle by t = 9 min.

Movie S3. The mechanical configuration of the synapse is established in ~5 minutes. OT-1 CTLs transduced retrovirally with Lifeact-eGFP were combined with 300-Pa DAAM particles bearing surface H-2K^{b}-OVA and ICAM-1, and imaged every 3 minutes (video is 360×). Top left, a Z-projection of the fluorescence imaging data. Lifeact-eGFP is shown in green and the DAAM particle in magenta. Time in minutes is indicated. Top middle: world-map projection of particle shape. x- and y-axes are the polar angles theta and phi, respectively (see Fig. 1C). Red zones represent particle compression against the blue background, which indicates the unindented particle radius. Top right: Topographic map of the particle. Positive and negative curvature are denoted by blue-green and gold, respectively. Bottom row: cross-sectional outline (left) and radii

about the cross section (right), showing particle compression and texturing. Contact begins at t = 0 min, and full compression is effected on the DAAM particle by t = 6 min.

Movie S4. Degranulation and target micropatterning are coordinated in space and time. OT-1 CTLs transduced retrovirally with Lamp1-eGFP were combined with 300-Pa DAAM particles bearing surface anti-CD3ε (145-2C11) and ICAM-1, and imaged every minute (video is approx. 300× before pausing). Left: a Z-projection of the fluorescence imaging data. Lamp1-eGFP is shown in green and the DAAM particle in magenta. Time in minutes is indicated. Middle: *En face* view of CTL lytic granules, defined by taking the Lamp1-eGFP signal within 500 nm of the target DAAM particle. Right: *En face* view of the DAAM particle topography. Positive and negative curvature are denoted by blue-green and gold, respectively. At t = 19 min, the movie pauses to highlight a degranulation event, defined by the next-frame loss of green signal both in the *en face* Lamp1-eGFP view and in the Z-projection of the movie.